International Journal of Automotive Technology, Vol. 7, No. 7, pp. 763–768 (2006)

1229–9138/2006/031–01

IDLE PERFORMANCE OF AN SI ENGINE WITH VARIATIONS IN ENGINE CONTROL PARAMETERS

D.-S. KIM and Y.-S. CHO*

Graduate School of Automotive Engineering, Kookmin University, Seoul 136-702, Korea

(Received 6 January 2006; Revised 18 September 2006)

ABSTRACT–Emission reduction in the cold start period of SI engines is crucial to meet stringent emission regulations such as SULEV. Emissoin reduction is the starting point of the study in the which the variable valve timing (VVT) technology may be one promising method to minimize cold start emissions while maintaining engine performance. This is because it is possible to change valve overlap and residual gas fraction during cold start and idle operations. Our previous study showed that spark timing is another important factor for reducing cold-start emissions since it affects warm-up time of close-coupled catalysts (CCC) by changing exhaust gas temperature. However, even though these factors may be favorable for reduction of emissions, they may deteriorate combustion stability in these operating conditions. This means that the two variables should be optimized for best exhaust emissions and engine stability. This study investigated the effects of valve and spark timings in idle performance such as combustion stability and exhaust emissions. Experiments showed that valve timings significantly affected engine stability and exhaust emissions, especially CO and NO_x, due to change in residual gas fraction within the combustion chamber. Spark timing also affects HC emissions and exhaust gas temperature. Yet it has no significant effects on combustion stability. A control strategy of proper valve timing and spark timing is suggested in order to achieve a reduction in exhaust emissions and a stable operation of the engine in a cold start and idle operation.

KEY WORDS : Idle operation, Spark timing, Exhaust valve timing, Exhaust emission, Combustion stability

1. INTRODUCTION

Three-way catalyst (TWC), the successful application of the emission after-treatment of SI engines, is very effective in lowering the emission levels from vehicles. The conversion rates of CO, HC and NO_x of a TWC are very high above 90%, after fully activated. However, it also has inherent problems related to catalytic chemical reactions. Since the catalyst stays at lower temperatures during a cold start period, harmful species such as CO and HC pass through the TWC without catalytic reaction, and the level of exhaust emissions becomes very high in this period. Therefore, the key technologies to meet the stringent emission regulations such as LEV, ULEV and SULEV of CARB, and to protect the air quality in urban areas are closely related to reduce the time required to reach the light-off temperature of a catalysts in the cold start period (Summers *et al.*, 1993; Cho and Kim, 2004, 2005; Lee *et al.*, 2004).

Previous studies showed that changes in spark ignition timing significantly affect exhaust gas temperature in cold start period (Russ *et al.*, 1999). When spark ignition timing is retarded, the start of combustion is delayed, resulting in a lower maximum cylinder pressure. On the other hand, flame stays up to a later stage of the expansion stroke and the exhaust gas temperature is higher than that of the normal spark ignition. Although energy loss is considerable with retarded spark timing, rapid warm-up of catalyst in a cold start period can be achieved from an increase in the exhaust gas temperature. Recent developments in engine control unit (ECU) and variable valve timing (VVT) technology are also very helpful in minimizing the warm-up time of catalysts in cold start. A VVT system can change the intake or exhaust valve timings to optimize the gas exchange processes. The engine operating parameters such as engine speed, load and coolant temperature change according to changes in VVT (Charles and Stanglmaier, 1999). In general, VVT is applied to improve the torque of an engine by virtue of the increase of volumetric efficiency in full-load and operation. These days, VVT is also efficient in improving the fuel economy and NO_x reduction due to the changes in residual gas of a combustion chamber. It is a crucial reason why some studies focus on the effects of residual gas with VVT operations (Kwak *et al.*, 2006). Changes in the intake and exhaust valve

*Corresponding author. e-mail: yscho@kookmin.ac.kr

timings affect flame speed and temperature mainly due to residual gas fraction in the cylinder. These changes handle the combustion processes directly. Therefore, it is anticipated that a proper change in valve timing can also raise the exhaust gas temperature for rapid warm-up of the catalysts in the cold start period.

However, such changes in spark and valve timings can affect the combustion stability that leads to poor idle quality and emission compositions. It would be meaningless if exhaust temperature increased with a sacrifice in combustion stability resulting in the increase of harmful emissions. Therefore, a proper change in these timings should result in higher exhaust temperatures while maintaining or improving stability and exhaust emissions.

The main objectives of this study are to find out the effects of the spark ignition timing and exhaust valve timing on both engine stability and exhaust gas composition. In this study, the effects of exhaust valve timing and spark ignition timing on idle operation are investigated through engine bench tests. Exhaust valve timing is changed using a variable timing camshaft, and spark ignition timing is changed using an external ECU. The changes in combustion characteristics and exhaust gas composition are measured and analyzed under various spark and valve timing conditions. In addition, the variations of combustion stability with the change in these timings are also investigated.

2. EXPERIMENTAL SETUP

2.1. Measurements

A 2-liter, naturally aspirated, four-cylinder SI engine is used as a test engine. Table 1 describes specifications of the engine. Figure 1 shows a schematic diagram of the experimental setup. A piezoelectric pressure transducer (Kistler, 6052B) measures pressure change in cylinder #1 in which a spark-plug type mount is installed. Measuring timings are synchronized with the crank angle encoder that generates pulses at every 0.1 degree of crank angle. Therefore, 7200 pressure data are acquired in one cycle of cylinder #1 and it is sufficient for assessments of cyclic variations through indicated diagrams (Heywood, 1988). Measured pressure charges are converted to voltage signals by a charge-to-voltage amplifier and acquired by a data acquisition system (National Instruments, DAQCard-MIO-16E4 and BNC-2090). An absolute pressure sensor (Kistler, 4045B) measures pressure in the intake plenum chamber for the calibration of drift effects of the pressure transducer. The data acquisition system also measures signals from TDC sensor of the engine in the same manner to determine where the top center is located on pressure curves.

Table 1. Specifications of test engine.

Items	Specifications
Type	4 cylinder, Spark-ignition, In-line, DOHC
Bore	82 mm
Stroke	93.5 mm
Compression ratio	10.1
Idle speed	700±100 rpm
Spark timing on idle	BTDC 8°±5°
Intake valve timing	BTDC 9°/ABDC 43°
Exhaust valve timing	BBDC 50°/ATDC 6°
Valve overlap	15°

The measured pressure data is applied to measure the coefficient of imep variation (COV_{imep}), which is an index to evaluate combustion stability. A PC-based combustion analyzer using LabVIEW collects the data and calculates COVs. At first, in order to obtain p-θ diagrams from voltage signals, the analyzer calculates absolute cylinder pressure from voltage signals, intake pressure and scale factor of the amplifier. After that, the analyzer calculates cylinder volume from synchronized crank angles in each cycle to obtain P-V diagrams. Engine specifications and measurement conditions should be supplied for the consequent operations. Numerical cyclic integrations are carried out from P-V curves to find imep of each cycle. These imep values are statistically evaluated for the COV_{imep} with Equation (1).

$$COV_{imep}=\frac{\sigma_{imep}}{imep}\times 100(\%) \quad (1)$$

An exhaust gas analyzer (Horiba, EXSA-1500) is used to measure exhaust gas compositions. It measures the concentrations of CO, HC and NO_x, and then calculates air-fuel ratio from measured data, applying it to the Spindt equation. Changes in engine control parameters

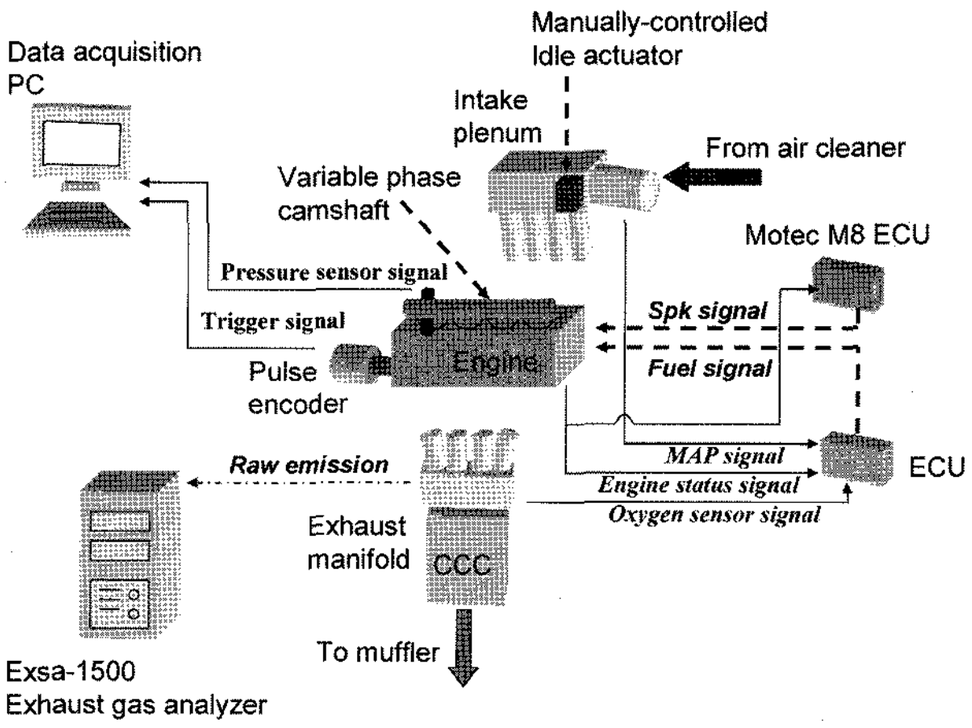

Figure 1. Schematic diagram of experimental setup.

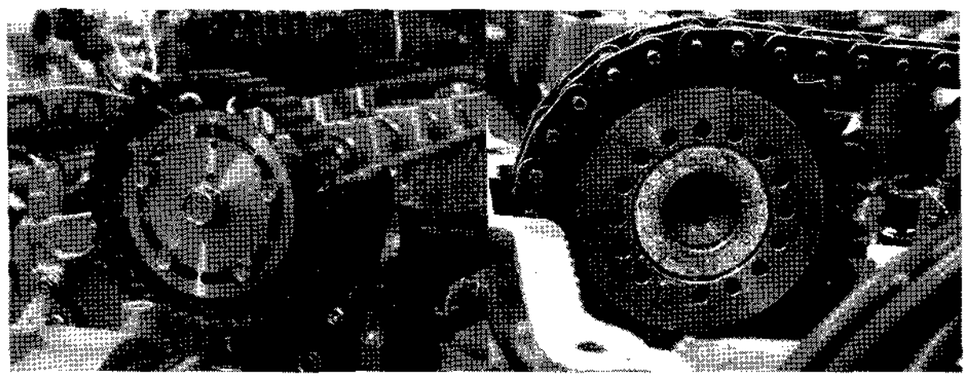

Figure 2. Variable timing camshaft mounted on test engine.

lead to the change in exhaust gas composition. However, the effects become smaller after exhaust gas passes through the catalyst. Therefore, as shown in Figure 1, a sampling probe is installed at the end of exhaust manifold to measure engine-out emissions.

2.2. Controls of Valve and Spark Timing

In the test engine, a variable timing camshaft that can change the phase of cam events is installed for the control of exhaust valve timings. Figure 2 shows the variable timing camshaft mounted on the test engine and modified sprocket for the experiments. The cam sprocket and chain pulley can be disassembled from the camshaft while the engine is on the test bench. Exhaust cam phase can be changed by simply turning the camshaft when the sprocket and pulley are disconnected. As shown in Figure 2, there are 16 keyholes on the pulley. On the camshaft mount, there are 15 keyholes. Consequently, the minimum change in cam phase is 3 degrees of crank angle.

Generally, exhaust compositions are very sensitive with the change in air-fuel ratio. In a conventional engine, engine management system (EMS) controls various engine parts such as the idle speed actuator (ISA), fuel injector, and ignition system. In this study, we needed to handle only the ignition system without changing other conditions that may affect air-fuel ratio. Furthermore, the change in spark timing leads to variations in engine torque. In an idle condition, engine speed is very sensitive to the change in spark timing.

At first, the original ECU (ECU #1) normally communicates with every sensor and actuator of the engine while a programmable ECU (Motec M8; ECU #2) receives data from a crank angle sensor and a TDC sensor. These are crucial to determine and control spark timing. The ECU #2 supplies spark signals to the ignition system. At the same time, spark signals from ECU #1 are supplied to a dummy ignition system in order to prevent the malfunction of OBD system. Spark timings of ECU#2 are determined by an external control PC. In this way, it is possible to control the ignition system as an open-loop circuit while maintaining other parameters controlled by ECU #1. However, the ISA is still under control of ECU #1 and there is no way for the ECU #1 to realize such change in spark timings. In preliminary tests, it was found that the open-loop control of spark timing caused the ECU #1 to control the ISA abnormally in order to maintain engine stability. To solve the problem, a manually-controlled idle actuator with a small valve was used instead of the ISA. The valve is widely open when the engine is cranking, and the degree of valve opening is handled manually to set the same engine speed in every test condition.

2.3. Test Conditions

In this study, measurements are performed after coolant temperature of the engine exceeds 82.5, the criterion of steady-state operation. The timings of exhaust valve open (EVO) are: BBDC 50°CA for the baseline case, BBDC 53 to 62°CA by 3°CA for the advanced cases, and BBDC 47 to 38°CA by 3°CA for the retarded cases. The numbers of crank angle increase when the timings are advanced and then decrease when they are retarded. The overlap period also increases when the EVO is advanced, and decreases with a retarded EVO. Therefore, the changes in crank angle differences are indicated as positive when advanced and negative when retarded. At each condition of EVO, spark timings are changed from BTDC 15 to ATDC 3°CA at an interval of 3°CA. The idle valve is controlled to maintain the engine speed at 900 rpm under each test condition. The actual range of engine speed was 900±30 rpm. Cylinder pressure curves of 30 consecutive cycles are captured for one measurement. This process is repeated ten times. In the same way, exhaust gas measurements are also repeated ten times. The representative values shown in the following figures are averages of each test condition.

3. RESULTS AND DISCUSSIONS

3.1. Combustion Stability

Figure 3 shows distribution of COV_{imep} with respect to changes in spark and EVO timings. It is clear that the COV_{imep} depends on changes in EVO rather than changes in spark timings. The primary reason of this phenomena can be explained as the change in valve overlap period. When using the variable timing camshaft, it is possible to change the exhaust valve open and close timings. Yet, these is no way to change the cam profile. This means that when the valve open timing is retarded or advanced, the valve close timing should be changed accordingly. Only the exhaust valve timing is changed in this experiment. The intake/exhaust valve overlap period should be altered because there is no change in intake valve timing. During idle operation of an SI engine, pressure in the intake manifold is much lower than that in the exhaust manifold. This causes a backward flow of exhaust gas during the valve overlap period and increases the amount

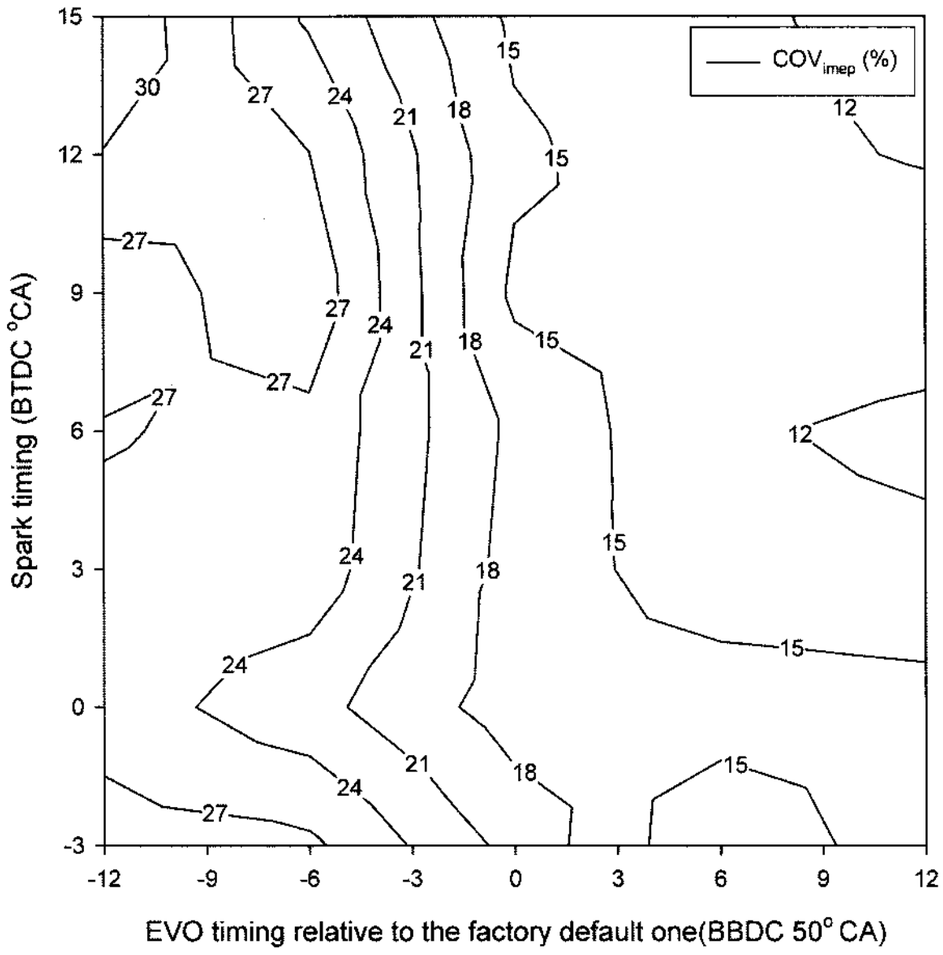

Figure 3. Distributions of COV_{imep} with respect to spark and EVO timings.

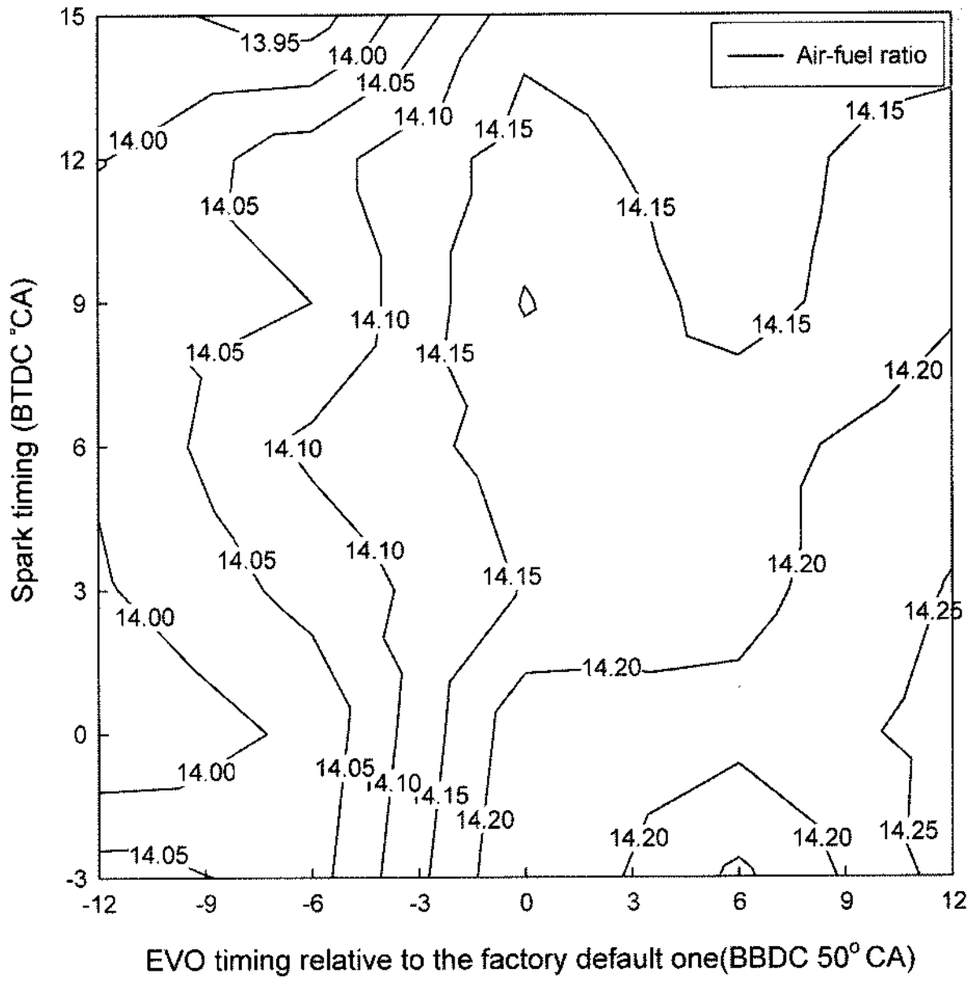

Figure 4. Distribution of air-fuel ratio with changes in spark and EVO timings.

of residual gas in the next cycle (Russ *et al.*, 1999b). When the exhaust valve timing is advanced, the overlap becomes shorter. On the contrary, when the exhaust valve timing is retarded, the overlap becomes longer. Therefore, changes in EVO lead to durations in valve overlap and increases in the amount of residual gas. The lower flame speed and engine stability occur when the residual gas fraction becomes higher especially in idle conditions. Figure 3 also shows that the changes in spark timings have no strong influences on variations in COV_{imep}. Small changes due to spark timings occur when EVO is extremely retarded or advanced.

In these tests, values of COV_{imep} are very high compared to part-load or full-load conditions. There are two difficulties in controling the engine. One difficulty is that the critical control of engine speed is hard, due to the open-loop setup of the amount of air through the ISA. The variations in engine speed may be one of the major reasons for the high COV_{imep}. The other difficulty is that there is no torque control due to the idle operation. The engine torque at idle is balanced by the friction of moving parts of the engine. Also, the rate of torque variation is relatively high in idle operation. It may cause the change in pressure in the cylinder. Imep variations are between 0.8–1.2 bar in the tests.

3.2. Emission Levels

As mentioned before, emission concentrations depend on air-fuel ratio. In this study, the ECU #1 controls the amount of fuel using a feedback loop with oxygen sensor. In idle, the coolant temperature is a major parameter whether the amount of fuel is controlled with a feedback loop or not. The coolant temperatures in each condition is above 82.5°C and the amount of fuel is in feedback control. Measurements of excess air ratio through an exhaust gas analyzer were about 0.95–0.96 in each condition. However, actual air-fuel ratio varied with respect to changes in test conditions. Figure 4 shows the distribution of air-fuel ratio with changes in test conditions. The

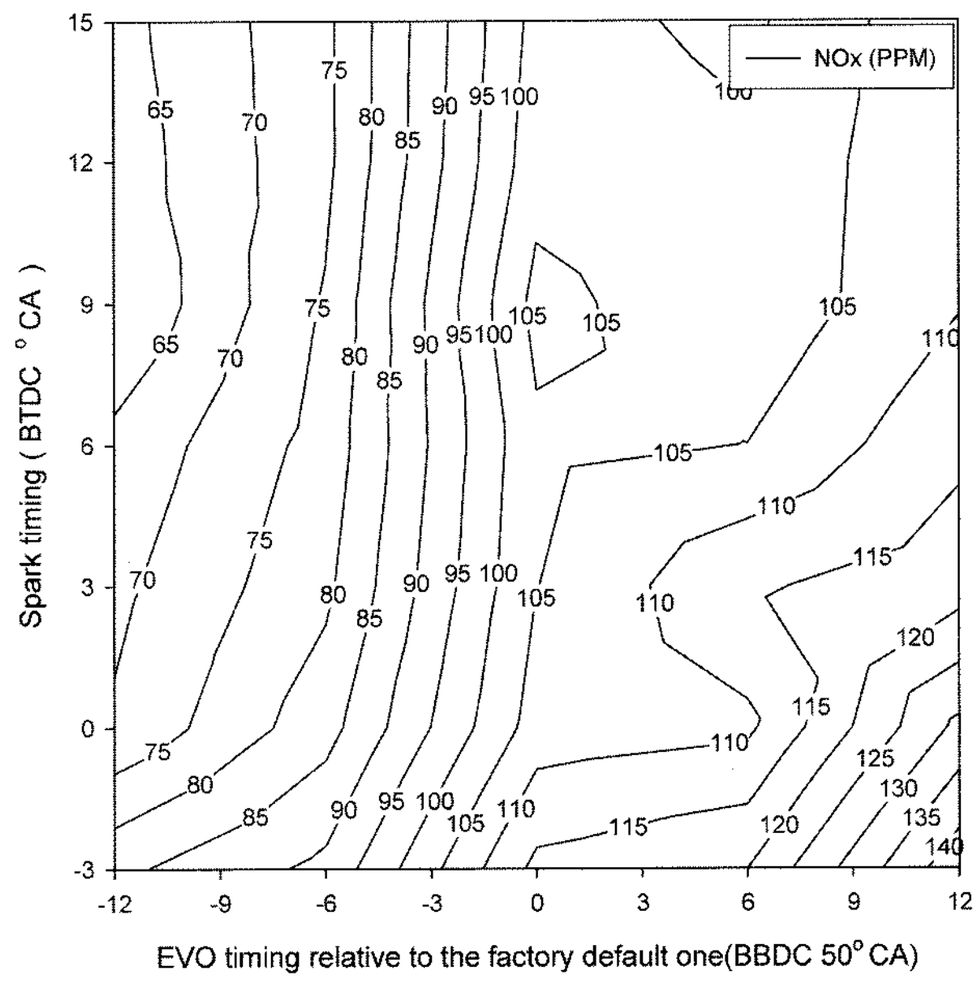

Figure 5. Distribution of CO concentration with changes in spark and EVO timings.

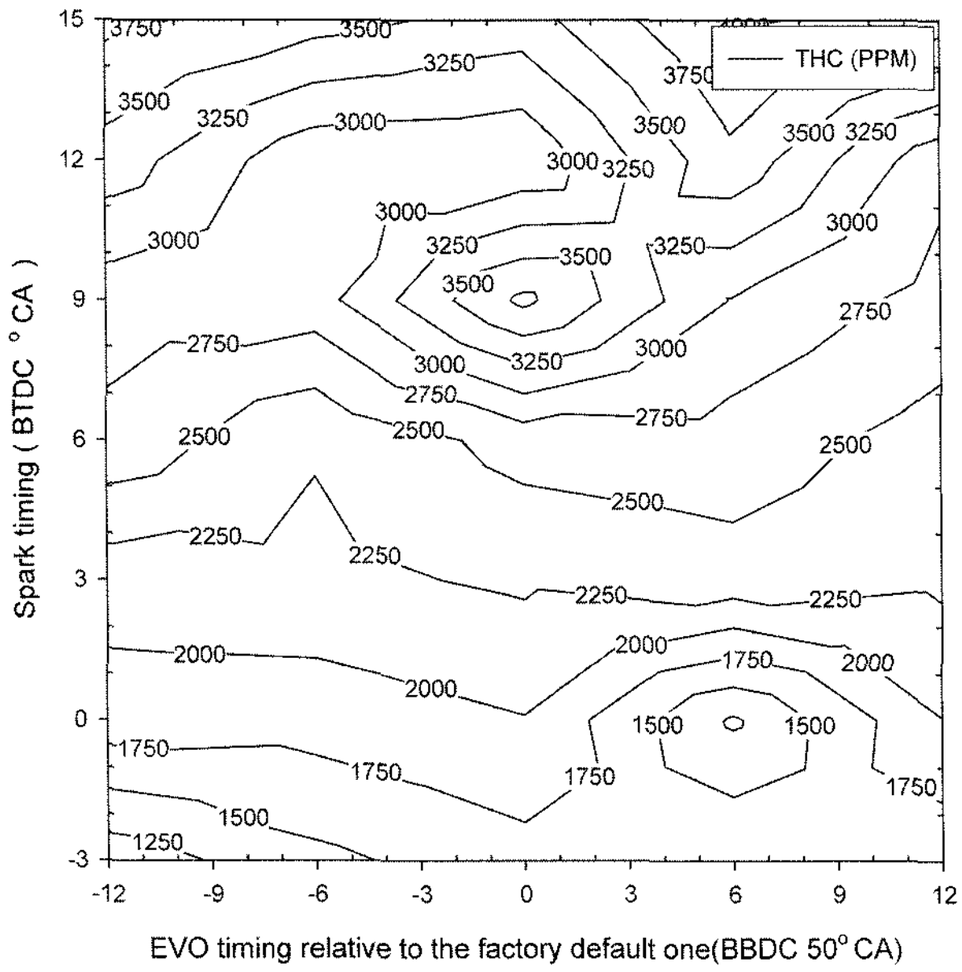

Figure 6. Distribution of NO_x concentration with changes in spark and EVO timings.

variations in air-fuel ratios are from 14.0 to 14.25 with air-fuel ratio varying slightly with changes in EVO. Spark timings show little effects on air-fuel ratio. The ranges of air-fuel ratio were near stoichiometric and the variation was similar when emission species are sampled at the end of the catalyst in the same test condtions.

The change in residual gas fraction in the cylinder may be the most crucial reason for the slight variation. However, emission concentration of CO is very sensitive to the amount of fresh air. Such change in air-fuel ratio would result in the variation of CO emissions. Figure 5 indicates this situation. Patterns of contour in Figure 4 and Figure 5 are very similar. Therefore, it is considered that the change in CO concentration with respect to EVO results from the dilution of residual gas, mainly due to the backflow during valve overlap period. These two figures also indicate that the effects in spark timings are relatively weak compared to the effects of EVO.

Figure 6 shows NO_x concentration with respect to the changes in test conditions. It is clear that the concentration of NO_x decreases when the EVO is retarded. In SI engines, NO_x emissions depend on the temperature of the burned gas. When the EVO timing is retarded, residual gas fraction increases due to the increase of valve overlap period. Such residual gas is sometimes referred as internal EGR. Decreases in flame speed and increases in average specific heat are the representative effects of EGR. Therefore, the NO_x concentration depends on the EVO changes due to the change in residual gas fraction. COV variation in Figure 3 is also considered that the variation depends mainly on the change in residual gas fraction.

In Figure 6, spark timing is not a dominant factor that affects NO_x concentration, although the retarded spark timings slightly increase NO_x emissions, especially when the EVO timings are advanced. Figure 6 shows that the retarded spark timing increases the temperature in the cylinder under idle operation. At medium or high speed operations, retarded ignition from MBT timing causes a decrease in maximum flame temperature and cylinder pressure due to the expansion stroke of pistons. However, mean piston speed of idle operations is lower and flame stays longer in the expansion stroke when spark timings are retarded. Our previous study showed that retarded spark timings increase exhaust gas temperature due to the late appearance of maximum rate of heat release (Kim and Cho, 2005).

From these results, it is clear that variation of EVO changes residual gas fraction in the cylinder, and that there are two opposite effects on exhaust gas composition and the stability of combustion. Advanced EVO is effective in reducing COV_{imep} and CO, but also increases NO_x emission. The effects are similar to the effects of EGR. Especially, these factors may interact more strongly in idle operations. Therefore, the controls should be much more precise in idle and cold-start operations. In Figure 3, a sharp increase in COV_{imep} is observed when EVO is retarded from +3 ~ +6°CA. At the same time, CO concentrations are also observed to increase rapidly for the same settings of EVO. Therefore, advanced EVO at about 4–5°CA, which is BBDC 45–46°CA, is considered an optimal EVO timing of the test engine in terms of stability and CO emission. NO_x emissions should be

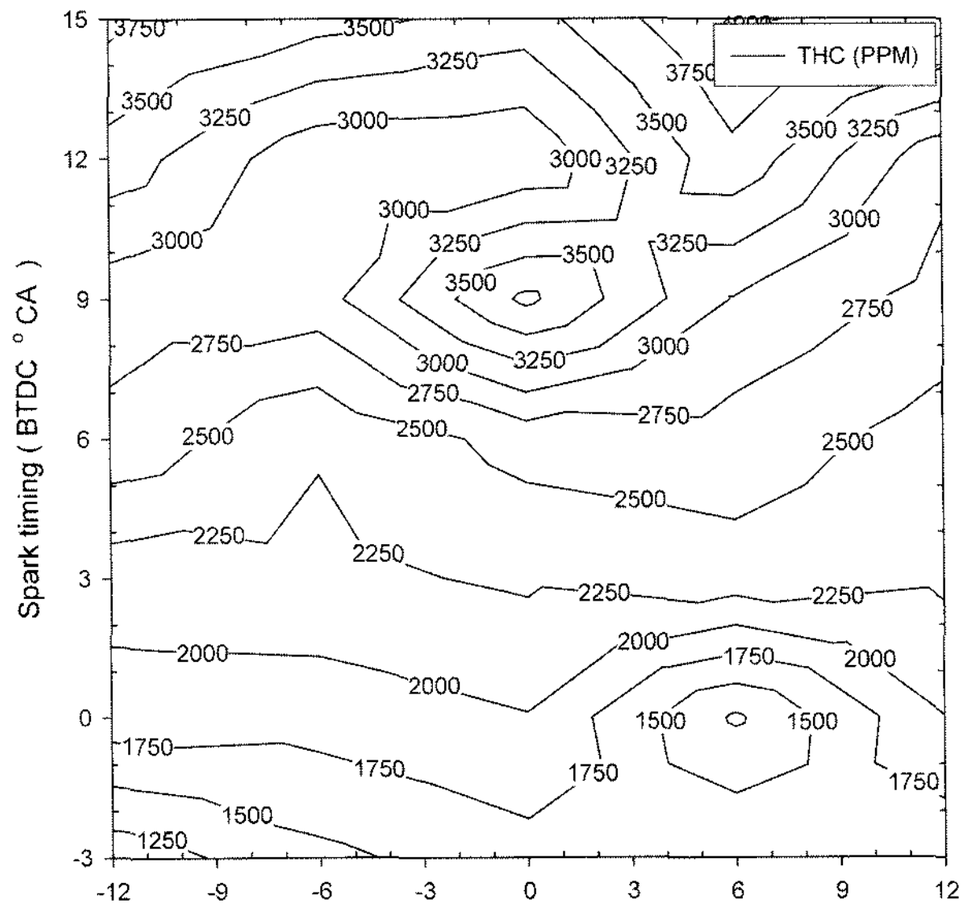

Figure 7. Distributions of THC concentration with changes in spark and EVO timings.

various crash situations on the dynamic response of the occupants is demonstrated by numerical simulations.

2. DYNAMIC RESPONSE ANALYSIS OF THE VEHICLE

Lumped mass models have been used since early 1970s for the analysis and design of automotive structures for safety during crash (Kamal, 1970). In these models, the major undeformable structural components are represented by lumped masses and the major deformable structural components are modeled as nonlinear spring elements, typically represented with the force-deformation data gained from experiments. Lumped parameter simulation has been employed for dynamic simulations and occupant analysis (Bennette *et al.*, 1991).

To predict the behavior of a vehicle involved in a head-on collision with another vehicle, the mathematical model shown in Figure 1 is used to obtain the dynamic response of the both vehicles.

In this model, the stiffness elements shown as springs with stiffness coefficients k_{ij} are the plastic deformation parts representing the longitudinal members in the front-end structure. The masses of the vehicle body and the bumper assembly are represented by M_{pi} and m_b, respectively.

The equations of motion of vehicle-to-vehicle frontal collision, as shown in Figure 1, can be written as the following equations.

$$M_{p1}\ddot{x}_{p1} + F_{11}(\delta_{11}) + F_{12}(\delta_{12}) = 0 \tag{1}$$

$$M_{p2}\ddot{x}_{p2} + F_{21}(\delta_{12}) + F_{22}(\delta_{22}) = 0 \tag{2}$$

$$m_b\ddot{x} + F_{21}(\delta_{12}) + F_{22}(\delta_{22}) - F_{11}(\delta_{11}) - F_{12}(\delta_{12}) = 0 \tag{3}$$

$$I_b\ddot{\theta}_b + F_{12}(\delta_{12})\cdot l_1 - F_{11}(\delta_{11})\cdot l_2 + F_{22}(\delta_{22})\cdot l_4 - F_{21}(\delta_{21})\cdot l_3 = 0 \tag{4}$$

where $\ddot{x}$ and $\ddot{x}_{p1}$ are the translation decelerations of the bumper assembly and passenger compartment (vehicle body), respectively. $\ddot{\theta}_b$ and I_b are the rotational deceleration and mass moment of inertia of the bumper assembly, respectively. l_i are the lengths between the plastic springs and the point (C.G) of rotation of the vehicle's bumper in offset collision.

The deformation of the plastic springs are given by

$$\delta_{11} = x_1 - x_{11},\ \delta_{12} = x_1 - x_{12} \tag{5}$$

$$\delta_{22} = x_2 + x_{22},\ \delta_{21} = x_2 + x_{21} \tag{6}$$

The displacements of the spring ends are defined as follows:

$$x_{11} = x + l_2\cdot\tan\theta_b,\ x_{12} = x - l_1\cdot\tan\theta_b \tag{7}$$

$$x_{21} = x - l_3\cdot\tan\theta_b,\ x_{22} = x + l_4\cdot\tan\theta_b \tag{8}$$

The forces of the plastic springs $F_{ij}(\delta_{ij})$, as shown in Figure 2, are defined using piecewise nonlinear functions in the displacement domain as follows:

$$F_{ij} = f_{0ij} + k_{ij}\cdot\delta_{ij} - F_{0ij} \tag{9}$$

where

$$k_{ij} = (k_{ij})_1,\ F_{0ij} = 0 \qquad \delta_{ij} \le \delta_{ij}^* \tag{9a}$$

$$k_{ij} = (k_{ij})_2,\ F_{0ij} = ((k_{ij})_2 - (k_{ij})_1)\cdot\delta_{ij}^* \qquad \delta_{ij} > \delta_{ij}^* \tag{9b}$$

where i=1,2 (i=1 represents the vehicle 1, and i=1,2 represents the vehicle 2). j=1,2 (i=1 represents the right longitudinal member, and j=2 represents the left longitudinal member).

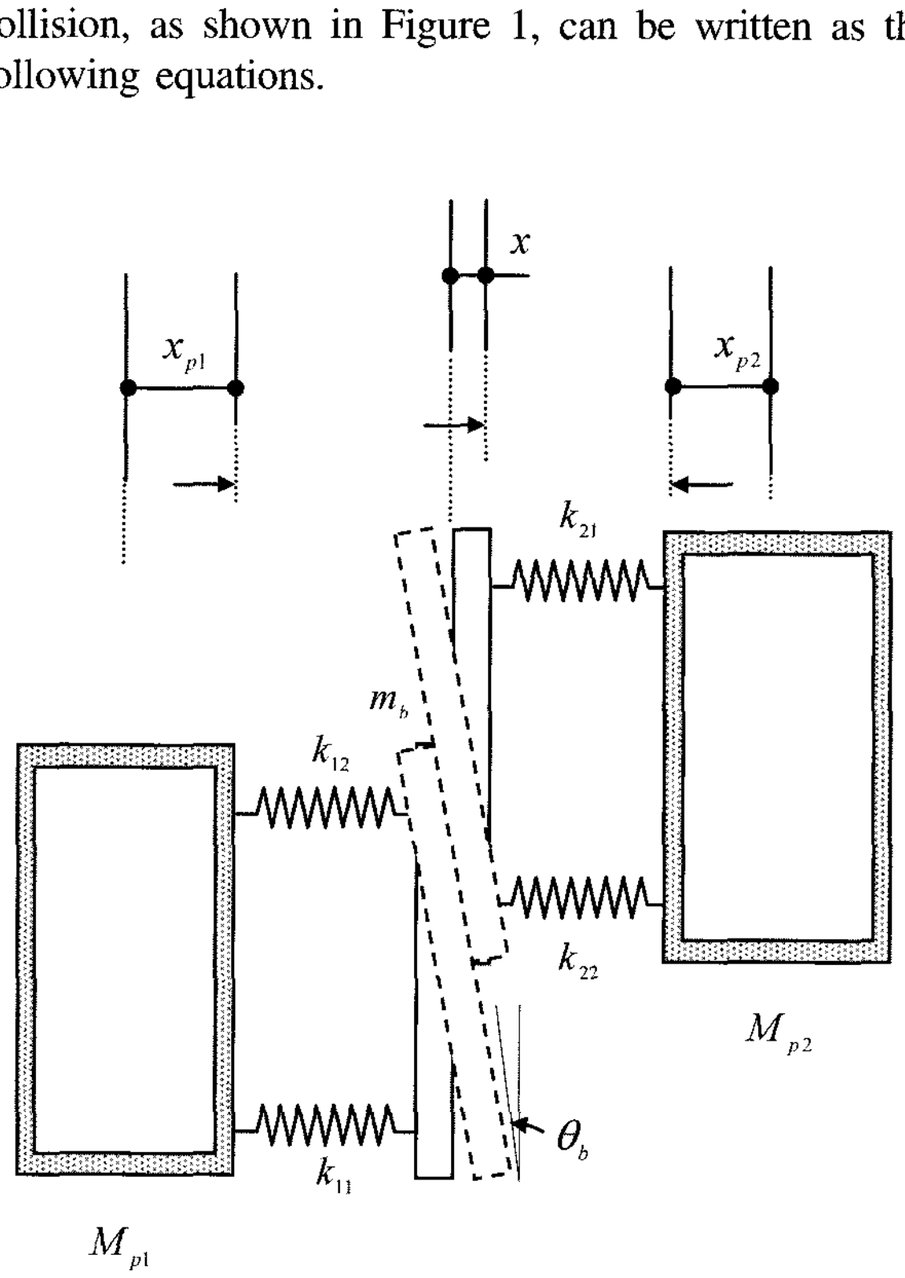

Figure 1. Vehicle-to-vehicle offset frontal collision.

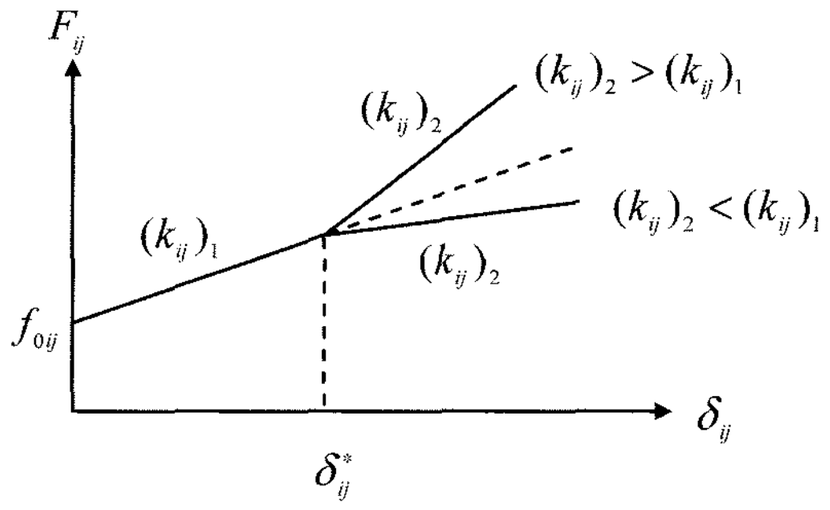

Figure 2. Force-deformation characteristics of the vehicle's longitudinal members.